Geophysical Journal International

Geophys. J. Int. (2012) **190,** 900–912 doi: 10.1111/j.1365-246X.2012.05558.x

Efficient full decay inversion of MRS data with a stretched-exponential approximation of the T_2^* distribution

Ahmad A. Behroozmand,[1] Esben Auken,[1] Gianluca Fiandaca,[1,2] Anders Vest Christiansen[1,3] and Niels B. Christensen[1]

[1] *Department of Geoscience, Aarhus University, Aarhus, Denmark. E-mail: ahmad@geo.au.dk*
[2] *Department of Mathematics and Informatics, University of Palermo, Palermo, Italy*
[3] *Geological Survey of Denmark and Greenland, Department of Groundwater and Quaternary Geology Mapping, Copenhagen, Denmark*

Accepted 2012 May 25. Received 2012 May 25; in original form 2011 September 16

SUMMARY

We present a new, efficient and accurate forward modelling and inversion scheme for magnetic resonance sounding (MRS) data. MRS, also called surface-nuclear magnetic resonance (surface-NMR), is the only non-invasive geophysical technique that directly detects free water in the subsurface. Based on the physical principle of NMR, protons of the water molecules in the subsurface are excited at a specific frequency, and the superposition of signals from all protons within the excited earth volume is measured to estimate the subsurface water content and other hydrological parameters. In this paper, a new inversion scheme is presented in which the entire data set is used, and multi-exponential behaviour of the NMR signal is approximated by the simple stretched-exponential approach. Compared to the mono-exponential interpretation of the decaying NMR signal, we introduce a single extra parameter, the stretching exponent, which helps describe the porosity in terms of a single relaxation time parameter, and helps to determine correct initial amplitude and relaxation time of the signal. Moreover, compared to a multi-exponential interpretation of the MRS data, the decay behaviour is approximated with considerably fewer parameters. The forward response is calculated in an efficient numerical manner in terms of magnetic field calculation, discretization and integration schemes, which allows fast computation while maintaining accuracy. A piecewise linear transmitter loop is considered for electromagnetic modelling of conductivities in the layered half-space providing electromagnetic modelling of arbitrary loop shapes. The decaying signal is integrated over time windows, called gates, which increases the signal-to-noise ratio, particularly at late times, and the data vector is described with a minimum number of samples, that is, gates. The accuracy of the forward response is investigated by comparing a MRS forward response with responses from three other approaches outlining significant differences between the three approaches. All together, a full MRS forward response is calculated in about 20 s and scales so that on 10 processors the calculation time is reduced to about 3–4 s. The proposed approach is examined through synthetic data and through a field example, which demonstrate the capability of the scheme. The results of the field example agree well the information from an in-site borehole.

Key words: Numerical solutions; Inverse theory; Electromagnetic theory; Hydrogeophysics.

INTRODUCTION

Nuclear magnetic resonance (NMR) has been developed in different branches of science since the 1930s. In the context of the earth's magnetic field, one of the fist reports was by Packard & Varian (1954). NMR has been applied in geophysics since the 1950s when saturated rock samples were studied in the laboratory. Surface-NMR is a non-invasive geophysical method applied to groundwater investigations. In the study of groundwater reservoirs from surface measurements, surface-NMR is unique among geophysical methods because it measures water content directly instead of indirectly relating a physical property (e.g. resistivity) to water content.

The initial amplitude and relaxation time of the surface-NMR decaying signal, the so-called free induction decay (FID), provide information of the investigated reservoirs: the initial amplitude is directly proportional to water content, and the relaxation time is related to pore structure and linked empirically to hydraulic conductivity (Kenyon 1997; Legchenko & Valla 2002; Mohnke & Yaramanci 2008).

Three major schemes exist for inversion of surface-NMR data: (1) the initial amplitude inversion (Legchenko & Shushakov 1998), which assumes mono-exponential behaviour of the relaxation and returns water content distribution using the extrapolated FID initial amplitudes, the so-called sounding curve (initial amplitude versus pulse moment); (2) the time step inversion, which separates the data set into different sounding curves and returns water-content distribution ($W(z,t)$) at different time steps t_n. One can then fit this structure by a mono-exponential curve (Legchenko & Valla 2002) and estimate the water content ($W(z)$) and relaxation time ($T_2^*(z)$) distributions, or use multi-exponential fit (Mohnke & Yaramanci 2005) leading to the partial water content distribution $W(z, T_2^*)$; (3) the QT inversion (Mueller-Petke & Yaramanci 2010) that considers the entire data set and inverts the data set directly for $W(z, T_2^*)$ (the 'Q' and 'T' refer to pulse moment and time, respectively).

In this paper, we introduce a new and simple scheme for inversion of the full surface-NMR data set, that is, the entire set of measured voltages in dependent of pulse moment, q and time, t, $V(q,t)$. Hence, from the data space point of view, the routine is similar to the QT approach. The multi-exponential behaviour of the NMR signal is taken into account and modelled by the stretched-exponential (SE) approximation to the data (Hilfer 2002), in which the time constant and stretching exponent determine the spectral information of the relaxation time distribution as described in the next section. In the following, we will describe the underlying assumptions for accurate approximation of the signal by the SE approach and its application in surface-NMR investigations. We have developed extremely efficient numerical implementations for magnetic field computation, discretization and integration. The accuracy of these implementations are presented and compared with reference responses, and with the three other approaches. Finally, we examine the scheme by showing both a synthetic example and a field example from Denmark.

METHODOLOGY

The physical property used in surface-NMR applications is the spin of hydrogen protons of water molecules in the subsurface. The nuclear spins are polarized in the static earth's magnetic field, which is relatively weak compared to most laboratory-NMR experiments. The weak field leads to a very small NMR signal, but the large investigation volume of the subsurface makes it possible anyway to measure the NMR signals using a wire-loop at the surface. The spin magnetic moment vectors precess about the static field at the Larmor frequency $f_{\mathrm{L}} = -\gamma B_0/2\pi$, ranging around 800–2500 Hz. In this expression, γ and B_0 denote the gyromagnetic ratio for the proton and the earth's magnetic field, respectively.

To excite the spins of the protons in the subsurface, an alternating current tuned at the Larmor frequency is passed through a large transmitter loop deployed on the surface. This energizing field forces the magnetization vector away from its equilibrium state along the static field. After the transmitter current is switched off, the protons will continue to precess while gradually reverting back to their equilibrium state; the lower level of energy. This precession produces an oscillating magnetic field, which induces a voltage response in the receiver loop. The voltage is a superposition of the signals arising from all the precessing nuclear spins within the excited earth volume (Weichman *et al*. 2000). To provide depth information, a series of measurements at increasing pulse moments, which is the product of current amplitude and pulse duration, $q = I_0\tau$, are passed through the loop. The larger the pulse moment, the larger the penetration depth.

The general forward expression of the QT surface-NMR signal is given by (e.g. Mueller-Petke & Yaramanci 2010)

$$V(q,t) = \int K(q,\mathbf{r}) \int W(\mathbf{r}, T_2^*) \mathrm{e}^{-\frac{t}{T_2^*}} \,\mathrm{d}T_2^* \mathrm{d}^3\mathbf{r}, \tag{1}$$

where $V(q,t)$ denotes the measured signal dependent on pulse moment (q) and time (t), $K(q,r)$ and $W(r, T_2^*)$ are the kernel function and partial water content (including multi-exponential information) and $\mathbf{r}$ is the position. Under on-resonance condition, and after decomposition of the elliptically polarized excitation field into two circular rotating parts, the kernel function becomes (Weichman *et al*. 2000; Hertrich 2008):

$$\begin{aligned} K(q,\mathbf{r}) = {} & \omega_L M_0 \sin\left(-\gamma \frac{q}{I_0} \left|\mathbf{B}_T^+(\mathbf{r})\right|\right) \frac{2}{I_0} \left|\mathbf{B}_R^-(\mathbf{r})\right| \mathrm{e}^{i[\zeta_T(\mathbf{r},\omega_L)+\zeta_R(\mathbf{r},\omega_L)]} \\ & \times \left[\hat{\mathbf{b}}_R^{\perp}(\mathbf{r},\omega_{\mathbf{L}}) \cdot \hat{\mathbf{b}}_T^{\perp}(\mathbf{r},\omega_{\mathbf{L}}) + i\hat{\mathbf{b}}_0 \cdot \hat{\mathbf{b}}_R^{\perp}(\mathbf{r},\omega_{\mathbf{L}}) \right. \\ & \left. \times \hat{\mathbf{b}}_T^{\perp}(\mathbf{r},\omega_{\mathbf{L}})\right], \end{aligned} \tag{2}$$

where ω_{L} is the angular Larmor frequency; I_0 and $\mathbf{r}$ represent transmitter loop current and position; $\hat{\mathbf{b}}_{\mathbf{0}}$, $\hat{\mathbf{b}}_{\mathbf{T}}^{\perp}$ and $\hat{\mathbf{b}}_{\mathbf{R}}^{\perp}$ are unit vectors in the direction of earth's magnetic field, and in the direction of perpendicularly projected transmitter and receiver fields to the earth's field, respectively; $B_{\mathrm{T,R}}^+(r)$ and $B_{\mathrm{T,R}}^-(r)$ denote co- and counter-rotating components of the elliptically polarized electromagnetic excitation field, perpendicular to the earth's field direction. The complex excitation field is decomposed in its elliptical components (α and β as minor and major axes of the ellipse, and the phase ζ). M_0 represents amplitude of the magnetization for protons in water at thermal equilibrium (net magnetization) given by Curie's law.

In 1-D applications, in which a horizontally stratified subsurface is assumed, the surface-NMR is referred to as magnetic resonance sounding (MRS), and typically the coincident loop configuration is used. Therefore, eq. (2) becomes

$$K(q,\mathbf{r}) = \omega_{\mathrm{L}} M_0 \sin\left(-\gamma \frac{q}{I_0} \left|\mathbf{B}_{\mathrm{T}}^+(\mathbf{r})\right|\right) \frac{2}{I_0} \left|\mathbf{B}_{\mathrm{T}}^-(\mathbf{r})\right| \mathrm{e}^{2i\zeta_{\mathrm{T}}(\mathbf{r},\omega_{\mathrm{L}})}, \tag{3}$$

and the 1-D NMR response is obtained by integrating eq. (1) over x and y

$$V(q,t) = \int K(q,z) \int W(z, T_2^*)\, \mathrm{e}^{-\frac{t}{T_2^*}} \,\mathrm{d}T_2^* \mathrm{d}z. \tag{4}$$

Multi-exponential evaluation of the full data set

The need to use the entire MRS data set is highlighted by Mueller-Petke & Yaramanci (2010) in which they examine and compare their QT results with the other schemes of using only the initial amplitudes or time step evaluation of the data. The measured MRS signal on a horizontally stratified subsurface containing multiple layers with varying relaxation times is inherently multi-exponential. Therefore, the relaxation of the MRS signal (FID) can be characterized by a broad distribution of decay time constants, each corresponding to a particular pore size structure (Dunn *et al*. 2002)

$$\frac{M(t)}{M_0} = \sum_{i=1}^{n} f_i \mathrm{e}^{-\frac{t}{T_{2i}^*}}, \sum_{i=1}^{n} f_i = 1, \tag{5}$$

where $M(t)$ and M_0 represent the magnetization at times t and 0, respectively; f_i is the volume fraction of the pores with a relaxation time T_{2i}^* and is proportional to the amount of hydrogen nuclei in that region; n denotes the number of different relaxation times.

Often the complexity of the physics of relaxation in layers of porous media is simplified using a mono-exponential model, but this—as we will show later—can lead to erroneous results. For NMR logging data, it was found that the solution to the non-linear inverse problem in eq. (5) was not adequate and, alternatively, the inverse problem can be reduced to a linear problem by assuming a set of relaxation times (T_{2i}^*) which are equally spaced on a logarithmic timescale and fitting for the amplitudes (f_i) only. This characterization forms the basis of the implementation presented by Mueller-Petke & Yaramanci (2010). Instead, we approximate the complex decay behaviour in terms of a 'stretched-exponential' or Kohlrausch relaxation function (Kenyon *et al*. 1986; Kenyon *et al*. 1988; Hilfer 2002). The *SE* approach was first introduced by Kohlrausch in 1847 by assuming a non-constant decay rate of the relaxation signal, and is widely accepted that the *SE* function describes a broad distribution of experimental data (Phillips 1996). This is a generalization of an exponential Debye relaxation function given by

$$\frac{M(t)}{M_0} = \exp\left[-\left(\frac{t}{T_2^*}\right)^C\right]. \tag{6}$$

The continuous distribution of relaxation times is described by two parameters: the time constant T_2^*, and the stretching exponent C. The C parameter is limited to values between zero and one. Although C has no strict physical basis, it characterizes the deviation of the signal attenuation from a mono-exponential behaviour. It is an indication of the homogeneity of the relaxation rate such that a value near one indicates an almost mono-exponential attenuation characteristic of the signal. When the stretching exponent becomes unity, eq. (6) reduces to a mono-exponential model. Therefore, the mono-exponential model is enclosed in the *SE* approach.

In petrophysical NMR, the *SE* function was suggested by Kenyon *et al*. (1988), in which they present the validity of the model and show that the *SE* fit the measured relaxation curves of numerous water-saturated sandstones samples. As a consequence, the *SE* representation provides a robust estimation of permeability, k, from borehole data using $k \propto \phi^4 T^2$, where ϕ is porosity and T is the relaxation time. This form has also been applied in MRS for estimation of permeability (e.g. Legchenko *et al*. 2002). However, there are also examples of relaxation data for petrophysical samples that the *SE* form does not fit well (Dunn *et al*. 2002). In the MRS application, the underlying assumption in using the *SE* formulation is that the relaxation distribution is mono-modal, meaning that the relaxation time distribution contains only one peak. In other words, as long as a strong non-exponential behaviour does not exist, the relaxation signal can be accurately approximated by the *SE* function (Peyron *et al*. 1996; Apitz & Johansen 2005). This assumption is generally valid in MRS because the measuring time interval of the MRS decays is relatively short, and the first data are typically measured after around 10–40 ms (Borgia *et al*. 1996; Peyron *et al*. 1996; Apitz & Johansen 2005).

The model is computationally simple, and the relaxation distribution is accurately approximated by only adding the parameter C to the mono-exponential modelling.

Fig. 1(a) shows a relaxation signal as a superposition of five different signals, each decaying as a mono-exponential with relaxation times T_i and with amplitudes f_i (eq. 5). The relaxation times are 40, 63, 100, 159 and 251 ms, respectively, with matching amplitudes of 0.15, 0.2, 0.3, 0.2 and 0.15. The resulting signal (circles) can be modelled by a stretched-exponential fit (black line, Fig. 1b) with an initial amplitude of 1.04, a relaxation time of 90 ms and a stretching exponent of 0.73. Fitting the data with a mono-exponential function (grey line, Fig. 1b) causes the relaxation time to be overestimated at 188 ms, and the initial amplitude to be underestimated at 0.51. The mono-exponential estimation has a residual of 17.47 per cent whereas it is 2.3 per cent for the stretched-exponential. In this example, it is therefore possible to characterize the resulting signal by three parameters (f, T, C) instead of 10 ($f_1, T_1, \ldots, f_5, T_5$). In other words, a multi-exponential function represents the signal equally well, but using many more parameters, which is undesirable from an inversion point of view where we strive to minimize the number of parameters to solve. In the next examples, we will not compare the results to a multi-exponential model as it is beyond the scope of this paper. A comparison with other conventional schemes is discussed in detail in Mueller-Petke & Yaramanci (2010).

In contrast to the mono-exponential model, the stretched-exponential approach provides a better estimation of both initial

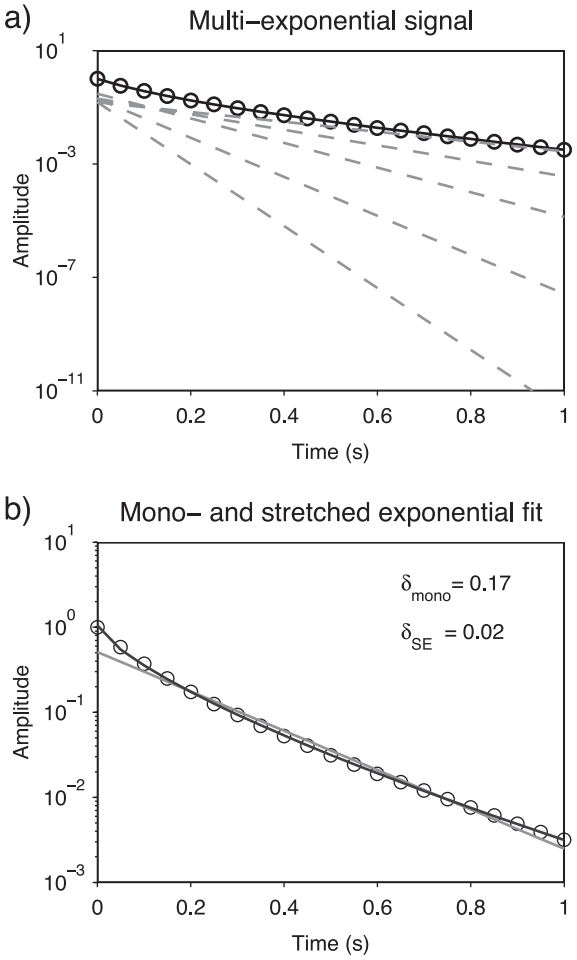

Figure 1. (a) A resultant relaxation signal (circles) as superposition of five different mono-exponential signals (dashed lines, logarithmic scale). The relaxation times are 40, 63, 100, 159 and 251 ms, respectively, with matching amplitudes of 0.15, 0.2, 0.3, 0.2 and 0.15, from bottom to top. (b) The signal is estimated by a stretched-exponential (black line) or mono-exponential (grey line) fit to the data.

amplitudes and relaxation times, and compared with the *QT* approach, fewer model parameters are used while the spectral information of the relaxation is still taken into account. Eventually, the parameters found in the inversion of MRS data are used to estimate hydraulic properties of the subsurface, and the question is whether information is lost by describing the decay through the parameter, C, instead of keeping all the spectral coefficients, f_i, in eq. (5). In our opinion, nothing is lost. First of all, the coefficients are not well determined anyway (Peyron *et al*. 1996), and, secondly, the estimation of hydraulic properties from MRS parameters is basically empirical using expressions containing *ad hoc* constants valid only over a limited hydraulic regime. By estimating much less model parameters, the parameters of the stretched-exponential approach are better determined in the inversion of MRS data than the spectral coefficients.

Using a stretched-exponential approximation, eq. (4) becomes

$$V(q,t) = \int K(q,z)\, W(z) f\left[T_2^*(z), C(z)\right] \mathrm{d}z, \tag{7}$$

in which

$$f\left[T_2^*(z), C(z)\right] = \exp\left\{-\left[\frac{t}{T_2^*(z)}\right]^{C(z)}\right\}. \tag{8}$$

The model space for the 1-D forward response is then defined as

$$\mathbf{m} = \left(\rho_i, \mathrm{thk}_j, W_i, T_{2i}^*, C_i\right)^T \; i = 1, N_{\mathrm{Layers}}, \; j = 1, N_{\mathrm{Layers}} - 1, \tag{9}$$

where, in each layer, ρ and thk represent resistivity and thickness, W denotes water content, T_2^* is the mean relaxation time and C controls the width of distribution of relaxation time. The superscript T indicates vector transpose. The full model to be determined has $(N_{\mathrm{Layers}} \times 4) - 1$ parameters, assuming that resistivity structure is obtained by inverting, for example, TEM/DC resistivity data.

Efficient numerical implementation

In this section, we describe various numerical solutions that will be computationally efficient and provide an accurate forward response. First, we discuss the magnetic field computation. The field components are calculated for a piecewise linear loop laid out on a conductive layered half-space. Secondly, we consider the subsurface discretization and accurate integration of the MRS kernel. We provide the FIDs as time gates, which represent the decay characteristics of the response accurately and decrease the number of data considerably, contrary to using the full samples from the filtered signal. Finally, parallelization of the code is discussed, and a MRS forward response is compared with three existing approaches.

Magnetic field calculation

For electromagnetic modelling of conductivities in the layered half-space, we have used a piecewise linear loop as transmitter. This is an advantage of the routine compared to other approaches because it is possible to calculate the magnetic fields from an arbitrary shaped loop. The loop is defined by its apexes, and each wire segment is considered as a grounded wire source for which the field values are calculated at observation points in the subsurface. For any discretization point in the subsurface and for each segment of the loop, the coordinate system is rotated in such a way that the segment is centred at the origin and aligned along the x-axis. The magnetic field components at the observation point are then given by integrating the x-directed horizontal electric dipole expressions along the segment. Finally, the fields are rotated back to the original coordinate system. This procedure is repeated for all wire segments and the magnetic field components of the loop at any point are calculated by summing up the fields of all loop segments. The electromagnetic field of electric dipoles embedded in or above a stratified earth is fully described by, for example, Xiong (1989) and Wannamaker *et al*. (1984). Our field computations have been validated against those of *em1d* (by Ki Ha Lee, Lawrence Berkeley Laboratory) and the 1-D part of the integral equation code *em3d* (Wannamaker *et al*. 1984).

A source consisting of grounded wires can be considered as an electric dipole when the distance to the observation point is at least five times greater than the dipole length (Ward & Hohmann 1988). To ensure this, we set dipole lengths to 1/15 of the radial distance between the observation point and the grounded wire. This scheme allows the step length to be small when the transmitter is close to the observation point and large when the separation is large.

The upward- and downward-propagating plane waves of the magnetic field calculation only depend on the depth at which the observation point is located within the layered conductivity structure. Therefore, we calculate them once for each z-plane using the backward recurrence relation (Wannamaker *et al*. 1984), and then interpolate them through all discretization points in that plane. This will save computation time considerably as the recurrence relations are computationally expensive.

Discretization, cubic spline and accuracy

Great care must be exercised in the discretization to accurately represent the oscillatory nature of the MRS kernel function. In practice this implies sampling densely close to the wire and more sparsely far from the wire, and to appropriately discretize in the z direction. Dense equidistant sampling is not computationally feasible. In this paper and for the horizontal discretization of the MRS kernel form a square transmitter loop, we use the property of the hyperbolic sine function. It behaves linearly for small arguments and exponentially for large arguments, which meets our requirements. In each direction, by substituting x/y by $A\sinh(Bn)$ we sample equidistantly in n. This means that we discretize x/y equidistantly close to the wire and exponentially far from the wire. The model is fully described by two parameters A and B, which are determined by the smallest and the largest distance, and the number of intervals between. The discretization scheme is defined for the interval between the wire and loop centre in both the x- and y-direction (in the loop coordinate system) and extended systematically outside the loop (Fig. 2a).

To effectively interpolate the MRS kernel, we have used cubic splines. A spline constructed of piecewise third-order polynomials is passed and integrated through the set of kernel values at each direction (Forsythe *et al*. 1977). This reduces the number of samples as splines track the function effectively. To find the minimum number of samples required to get the desired accuracy, the response was calculated for a high number of samples between wire and loop centre and considered as reference. Then we recalculated the response by decreasing the number of points until we obtain an accuracy of 1 per cent with respect to the reference (Fig. 2b). For the typically used 50- and 100-m-side-square loop, we have found 30 as the minimum number of samples between wire and loop centre that will result in a response with an error below 1 per cent.

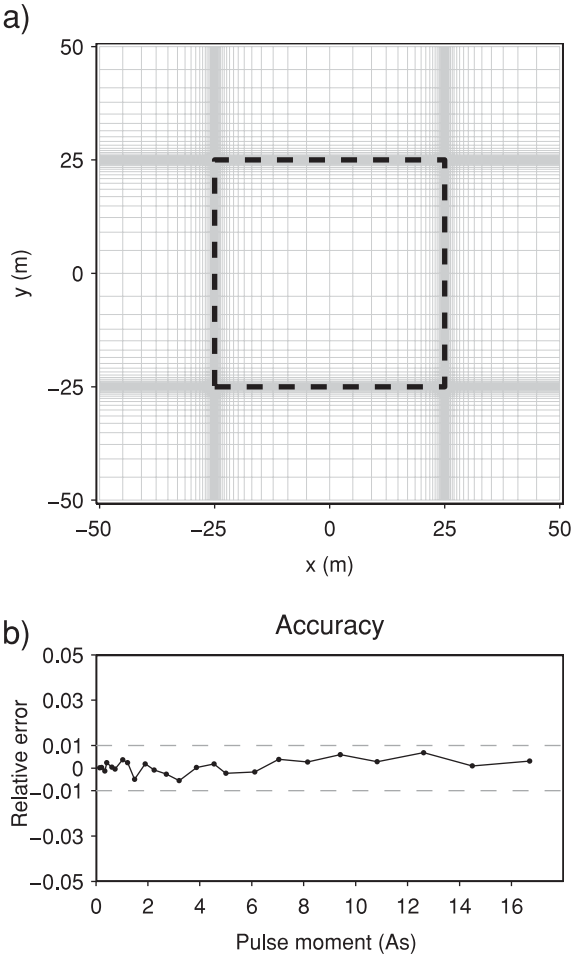

Figure 2. (a) Plane view of x/y discretization for a 50 m side-square loop based on the sinh function. (b) Accuracy of MRS response: relative error of MRS forward response using 30 points between wire and loop centre in comparison with true response (integration using cubic spline).

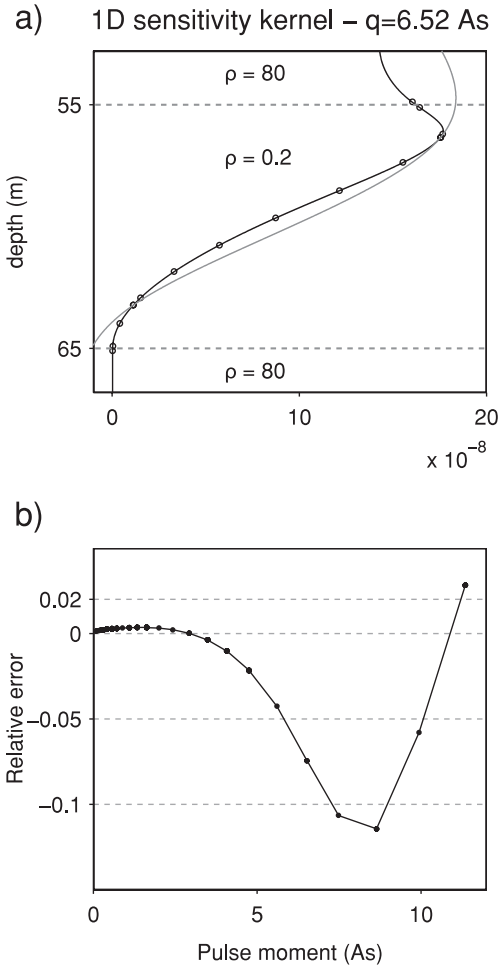

Figure 3. A close-up view of the resampling in z-discretization to provide accurate forward response. A 1-D MRS kernel is calculated using a 100-m-side-square loop over a three-layered earth. The layers have resistivities of 80, 0.2 and 80 ohm-m, respectively, and water content of 30 per cent. (a) Black circles show the discretization after resampling, black curve represents the kernel interpolated by the splines, and grey curve depicts the same kernel interpolated without resampling in the second layer. (b) The relative error in the forward response (difference between the two forward responses). The time axis is not shown because the errors do not vary with time.

Similarly, the MRS kernel function is highly oscillating with depth, and therefore, a well-chosen depth discretization is needed to obtain sufficient numerical accuracy. We have discretized the depth in a logarithmic manner and found 20 as a sufficient number of points per decade. Similar to the horizontal plane, the integration is done using cubic splines. The discretization is started from $z = 1$ cm, and the first decade (first 10 cm) is exceptionally discretized using 5 points. It is permissible due to the fact that this part has less sensitivity contribution because of its small volume fraction and, in most cases, negligible amount of water.

In addition, a search is done before each forward calculation to ensure a sufficient number of points in every layer. We consider the minimum number to be 10 points in each layer. If the layer has less than 10 points, it is resampled. Furthermore, to overcome discontinuities of the MRS kernel due to high resistivity contrast, two additional points are added just below and above each layer boundary. This discretization scheme helps the spline interpolation to track the function effectively. For instance, Fig. 3 shows a 1-D kernel distribution, from a 100-m-side-square loop deployed over a three-layered earth with resistivities of 80, 0.2 and 80 ohm-m, respectively. The pulse moment value is equal to 6.52 As. The high conductivity layer starts at 55 m and is 10 m thick. Based on the above-mentioned 20-points-per-decade discretization, only two points are assigned to the second layer. The grey curve in Fig. 3(a) shows the kernel function interpolated using these two points in the layer. For comparison, black dots in Fig. 3(a) represent the discretization points after resampling of the layer, ensuring minimum number of 10 points in the layer together with adding two points above and below each layer boundary for discontinuity consideration. The black curve represents the kernel function interpolated using the resampled points. Fig. 3(b) depicts the relative error in the forward response, that is, the difference between the two forward responses based on the two discretizations. We do not show the time axis in the plot because the errors do not vary with time. As the figure shows, the high resistivity contrast can introduce considerable error in the forward response, particularly through the pulse moments that have more sensitivity contribution to the second layer. All layers in the model have a water content of 30 per cent, so the difference in the forward response is solely due to the difference in the MRS kernel.

Fig. 4 illustrates a 1-D kernel, from a 50-m-side-square loop over a conductive layered half-space, for small (0.43 As, Fig. 4a) and moderate (3.49 As, Fig. 4b) pulse moment values. Grey curves show the reference 1-D kernel, which is calculated based on 100 points per decade, and represent the high variation of the kernel with depth. Black dots represent the same function discretized based on the above-mentioned 20-points-per-decade scheme, except for the top 10 cm which is sampled by five points. Despite high variation of the kernel function, splines interpolate and average the function well. To show that, the difference between the two forward responses (from the grey and red curves) is plotted as relative errors in Fig. 4(c), showing that the two forward responses are within 1 per cent of accuracy. Like in Fig. 3(b), the time axis is not shown here, and the difference is solely due to the difference in the MRS kernel. The discretization in layers of the few-layer model that we consider is much coarser. The kernel is integrated over the layers of the inverse problem (dashed lines at 5, 15 and 50 m depth) using integrated splines as described above.

Gate integration

The FIDs are integrated over gates reflecting an average of the measured voltage over the time windows. Gate integration is useful to increase signal-to-noise ratio, mainly at late times (Becker & Cheng 1988). Moreover, a smaller Jacobian is achieved for calculation of partial derivatives. As long as the time gates are densely sampled (e.g. ten points per decade), this can be done without any loss in the information contents of the data. In the forward calculations, as long as the gates are narrow compared with the delay time, it is a good approximation to the gate values to compute the signal in the geometric centre of the gate ($\sqrt{t_{\text{open}}t_{\text{close}}}$ where t_{open} and t_{close} denote the gate-open and gate-close times (Christiansen *et al*. 2011). Time gate filtering is beyond the scope of this paper.

Parallelization and speed

After the above-mentioned numerical implementations, the routine is computationally fast; the entire forward response is performed in about 20 s on one core (16 core; HP Proliant DL160 G6 system; 2 × Intel Xeon E5520 CPUs, 2.26 GHz 12 GB RAM; Hewlett-Packard Development Company, L.P., Houston, TX, USA). The code has also been optimized for parallel computation using Open MP, which is useful when computing on a single multi-CPU computer with a common local memory space for all parallel threads. The computation time is thereafter decreased to about 3–4 s on 10 cores. Parallelization saves computation time considerably when inverting the MRS data jointly with other geophysical methods (e.g. TEM) in which the forward response must be computed repeatedly for each resistivity update. Compared to the other available routines, the computation time is speeded up considerably.

Comparison with other approaches

For comparison of the presented approach with other routines, we had MRS forward responses (sounding curves) calculated using four different approaches; HGG (presented approach in this paper), MRSmatlab (computed by Mueller-Petke, private communication, 2012), Samovar (version 11×3; computed by Legchenko, private

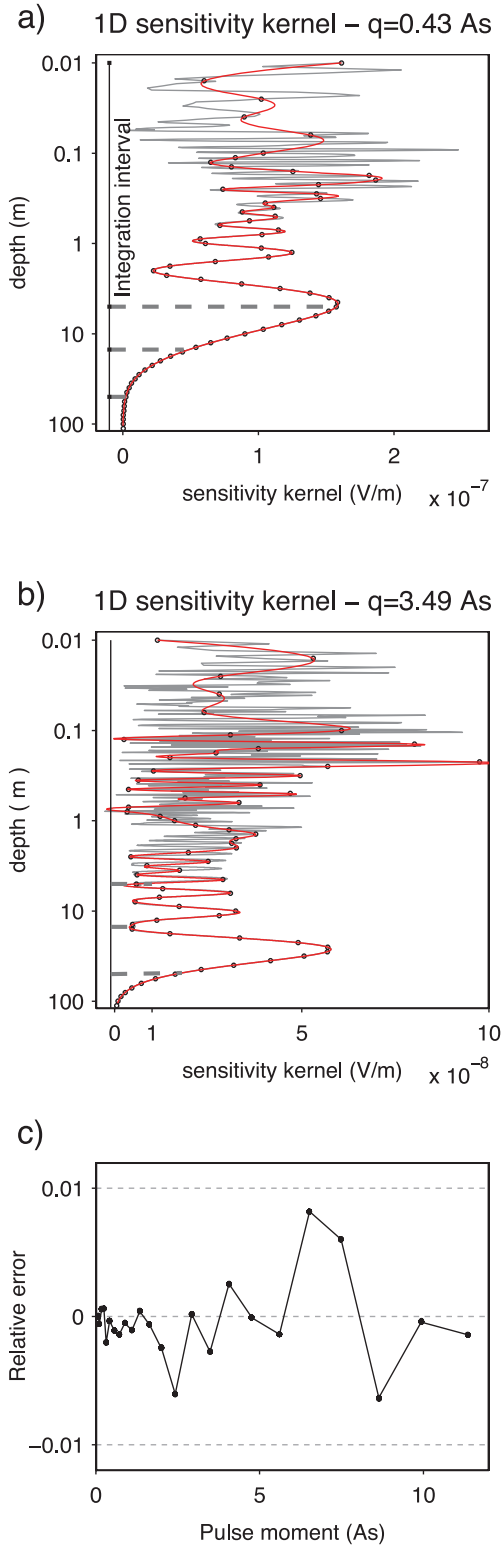

Figure 4. (a and b) 1-D kernel calculated using a 50-m-side-square loop over a conductive layered half-space with the layer boundaries at 5, 15 and 50m (dashed grey lines), for small (a) and moderate (b) q values. Grey curves represent the reference function based on 100-points-per-decade discretization, and red curves show the same function sampled by 20 points per decade. (c) Accuracy of 1-D MRS forward response (red curves in a and b) in comparison with the reference one (grey curves in a and b).

Table 1. Site specifications and characteristics of the discretization and computation schemes used for comparison of MRS forward responses of four different approaches. N_Z denotes number of discretization points in z-direction. The results are shown in Fig. 5.

	Description
Site specifications	Model parameters Resistivity: 50/200/20 ohm-m Thickness: 10/15 m Water content: 100 per cent, all layers
	Measurement Loop: Square, 100-m side, 1 turn Earth's field: Inclination, 70°, Declination: 0° Larmor frequency: 2100 Hz Temperature: 293 K
HGG	Discretization X/Y maximum: ±350 m Z minimum: 1 cm Depth sampling scheme: log + resampling of the layers if necessary + adding extra points for discontinuity (described in detail in the text), N_Z: 86
	Computation System: Intel Xeon E5520 CPU, 2.27 GHz Parallel computation: YES Time: 20 s (1 CPU), 3–4 s (10 CPU)
MRSmatlab	Discretization X/Y maximum: ±336 m, cylindrical coordinate system Z minimum: 2 cm Depth sampling scheme: loglin, starting with log, lin from 20 m (2-m spacing), N_Z: 102
	Computation System: Quad core AMD Phenom 9600B Parallel computation: NO Time: 675 s (1 CPU)
Samovar_11 × 3	Discretization X/Y maximum: ±500 m Z minimum: 10 cm Depth sampling scheme: automatic, based on Tx field gradient, N_Z: unknown
	Computation System: Intel® CoreTM i7 CPU X 920 @ 2 GHz, 7.92GB RAM Parallel computation: NO Time: 26 s (1 CPU)
IRIS	Discretization X/Y maximum: unknown Z minimum: 10 cm Depth sampling scheme: unknown, N_Z: 100
	Computation System: Intel® CoreTM 2 Duo CPU T 7250 @ 2 GHz, 1.95GB RAM Parallel computation: NO Time: 345 s (1 CPU)

communication, 2012) and IRIS (Samovar_7.0, supplied by NUMIS Poly equipment, IRIS Instruments, Orleans, France). The response is calculated for a 100-m-side-square loop, 1 turn, at Larmor frequency of 2100 Hz, earth's magnetic field inclination of 70° and declination of 0°, and at a temperature of 293 K. Table 1 shows the model and specifications together with discretization and computation characteristics of each routine. A three-layer conductivity structure is considered and a water content of 100 per cent is assigned to all layers so that the difference in forward responses will represent the difference in MRS kernel. HGG, Samovar and IRIS codes simulate the response using a square loop while MRSmatlab uses an equivalent circular loop of 112 m diameter for simulation. In z-direction, HGG and MRSmatlab discretize the earth from 1 and 2 cm, respectively, and Samovar and IRIS start at 10 cm; stated in Table 1. Fig. 5 shows the four responses in real and imaginary parts (a and b), followed by relative errors between the HGG response and other responses (c and d). A maximum pulse moment of 15.4 As is considered for the calculation of the forward response and the responses from MRSmatlab and IRIS are interpolated to the pulse moment values from HGG and Samovar, taken from a field data set acquired by the NUMIS Poly equipment.

For small pulse moment values, the real part of the responses (Fig. 5a) look similar, whereas a considerable difference is observed at larger pulse moments, especially compared to Samovar (Fig. 5c).

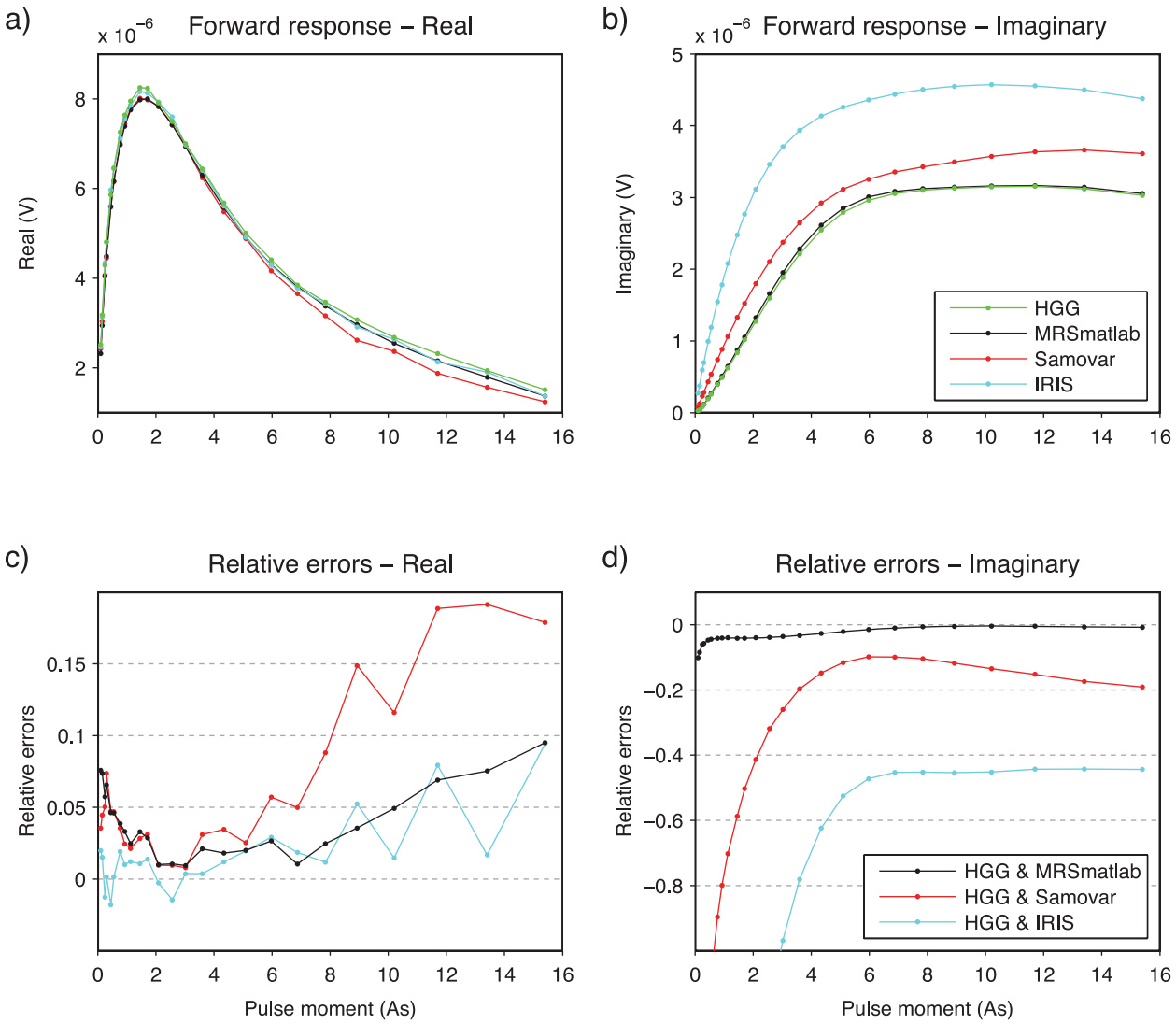

Figure 5. Comparison of MRS forward responses of four different approaches. (a) and (b) show real and imaginary parts, (c) and (d) show relative errors between the HGG (approach of this paper) and other approaches. Site specifications and characteristics of the discretization and computation schemes are mentioned in Table 1.

A significant difference is observed in the imaginary part (Fig. 5b), especially compared to the IRIS code and, to a lesser degree, the Samovar (Fig. 5d). This difference is larger at small pulse moments for all other codes.

INVERSION

The importance of considering the full data set and representing the decays by the stretched-exponential approach are discussed in the previous sections. All gated decays are included in the data space. In the model space, the spectral information of the relaxation times is approximated by the stretched-exponential approach as discussed earlier. In this paper, the 1-D forward response described by eqs (7) and (8) is directly used in the inversion. In contrast to the time step approach, the model parameters are obtained in one inversion procedure where the physical relationships between the model parameters are maintained.

To impose positivity, the logarithm of the data and model parameters are used in the inversion. Therefore, the model space becomes

$$\mathbf{m} = \left[\log(\rho_i), \log(\mathrm{thk}_j), \log(W_i), \log\left(T_{2i}^*\right), \log(C_i)\right]^T \quad i = 1, N_{\mathrm{Layers}}, j = 1, N_{\mathrm{Layers}} - 1, \tag{10}$$

and the data space contains the logarithm of the voltage at all gate centre times

$$\mathbf{d} = \left[\log(V_{i,j})\right]^T, \quad i = 1, N_q; \quad j = 1, N_{\mathrm{gates}}, \tag{11}$$

where N_q and N_{gates} represent the number of pulse moments and the number of gates, respectively.

The inversion approach fulfills the following demands.

(1) Accuracy of the forward response, implemented with all the features described in the previous section.

(2) Complete usage of the acquired data, considering all time gate values in the data space, which maintains the spectral information content.

(3) Description of the model using stretched-exponential approach; simple model description (compared to the *QT* approach), consider the spectral information contained in the time domain decays.

(4) Possibility of inverting for both layered and smooth models.

(5) The possibility of inverting more than one data set, either using lateral constraints (e.g. MRS soundings on a line), or mutual constraints (e.g. MRS inverted together with DC or TEM data).

(6) Computation of the sensitivity analysis of the model parameters.

Auken & Christiansen (2004) present a detailed description of the inversion algorithm. The methodology is only briefly outlined here. It follows the established practice of a linearized approximation of the non-linear forward mapping of the model to the data space, by the first term of the Taylor expansion

$$\boldsymbol{\delta d}_{\rm obs} = \boldsymbol{G}\delta \boldsymbol{m}_{\rm true} + \boldsymbol{e}_{\rm obs}, \tag{12}$$

where $\boldsymbol{\delta d}_{\rm obs}$ denotes the difference between the observed data and the non-linear mapping of the model to the data space, $\boldsymbol{\delta m}_{\rm true}$ represents the difference between the true model and an arbitrary reference model, $\boldsymbol{e}_{\rm obs}$ is observational error and $\boldsymbol{G}$ denotes the Jacobian matrix that contains the partial derivatives of the mapping.

The inversion follows an iterative updating scheme, where the model update $\boldsymbol{m}_{n+1}$ is obtained by:

$$\boldsymbol{m}_{n+1} = \boldsymbol{m}_n + \left[\boldsymbol{G}_n'^T \boldsymbol{C}'^{-1} \boldsymbol{G}_n' + \lambda_n \boldsymbol{I}\right]^{-1} \cdot \left[\boldsymbol{G}_n'^T \boldsymbol{C}'^{-1} \boldsymbol{\delta d}_n'\right], \tag{13}$$

where the Jacobian, $\boldsymbol{G}_n'$, the data vector update $\boldsymbol{\delta d}_n'$ and the covariance matrix, $\boldsymbol{C}'$ incorporate both the *a priori* and the roughness constraints and are defined as

$$\boldsymbol{G}_n' = \begin{bmatrix} \boldsymbol{G}_n \\ \boldsymbol{I} \\ \boldsymbol{R} \end{bmatrix} \tag{14}$$

$$\boldsymbol{\delta d}_n' = \begin{bmatrix} \boldsymbol{\delta d}_n \\ \boldsymbol{\delta m}_n \\ \boldsymbol{\delta r}_n \end{bmatrix} = \begin{bmatrix} \boldsymbol{d}_n - \boldsymbol{d}_{\rm obs} \\ \boldsymbol{m}_n - \boldsymbol{m}_{\rm prior} \\ -\boldsymbol{R}\boldsymbol{m}_n \end{bmatrix} \tag{15}$$

$$\boldsymbol{C}' = \begin{bmatrix} \boldsymbol{C}_{\rm obs} & 0 & 0 \\ 0 & \boldsymbol{C}_{\rm prior} & 0 \\ 0 & 0 & \boldsymbol{C}_{\rm R} \end{bmatrix} \tag{16}$$

In eq. (14), $\boldsymbol{G}_n$ represents the Jacobian of the forward mapping, $\boldsymbol{I}$ is the identity matrix with dimension $N_{\rm m} \times N_{\rm m}$, $N_{\rm m}$ being the number of model parameters and $\boldsymbol{R}$ is the roughness matrix which contains 1 and -1s for the constrained parameters, and 0 in all other places. The constraints are connected to the true model as $\boldsymbol{\delta m}_n = \boldsymbol{m}_n - \boldsymbol{m}_{\rm priori}$ and $\boldsymbol{\delta r}_n = -\boldsymbol{R}m_n$ and are added to the data vector update $\boldsymbol{\delta d}_n'$ (eq. 15). $\boldsymbol{\delta m}_n$ denotes the distance between the $n^{\rm th}$ model vector $\boldsymbol{m}_n$ and the *a priori* model vector $\boldsymbol{m}_{\rm prior}$, which is also used as a starting model for the iterative procedure, and $\boldsymbol{\delta r}_n$ is the roughness of the $n^{\rm th}$ model vector.

The covariance matrix $\boldsymbol{C}'$ of eq. (16) is defined in terms of the covariance of the observed data, $\boldsymbol{C}_{\rm obs}$, the covariance of the *a priori* information, $\boldsymbol{C}_{\rm prior}$ and the covariance of the roughness constraints, $\boldsymbol{C}_{\rm R}$. The first two of these matrices are diagonal; the elements of $\boldsymbol{C}_{\rm prior}$ and $\boldsymbol{C}_{\rm R}$ control the strength of the constraints, whereas the elements of $\boldsymbol{C}_{\rm obs}$ reflect the noise content of the data. As suggested in Tarantola & Valette (1982b), the error on the theoretical description of the forward response can be introduced in the inverse problem formulation through $\boldsymbol{C}_{\rm obs}$. Therefore, to account for the model dimensionality approximation, in the inversion scheme a minimum value for the diagonal elements of $\boldsymbol{C}_{\rm obs}$ is stated independently of the measured standard deviation. We suggest a minimum threshold for the standard deviation of 3 per cent on the data.

In eq. (13) the parameter λ is the Marquart damping factor (Marquart 1963), which is iteratively updated to stabilize the inversion process through an adaptive algorithm that damps the step size.

Eq. (13) minimizes the objective function expressed by

$$Q = \left[\frac{1}{N_{\rm d} + N_{\rm m} + N_{\rm C}} \left(\boldsymbol{\delta d}'^T \boldsymbol{C}'^{-1} \boldsymbol{\delta d}'\right)\right]^{\frac{1}{2}}, \tag{17}$$

in which $N_{\rm d}$, $N_{\rm m}$ and $N_{\rm C}$ denote the number of data points, the number of *a priori* constraints on the model parameters and the number of constraints. The output models are thus balanced by both the data and the *a priori* constraints and roughness constraints.

Finally, the covariance of the estimation error $\boldsymbol{C}_{\rm est}$ (Tarantola & Valette 1982a) is used to estimate the resolution of the inverted model by using its expression for linear mappings on the last iteration

$$\boldsymbol{C}_{\rm est} = \left(\boldsymbol{G}'^T \boldsymbol{C}'^{-1} \boldsymbol{G}'\right)^{-1}. \tag{18}$$

SYNTHETIC EXAMPLE

A full MRS data set has been simulated using a square loop with 50-m-loop sides deployed on a five-layer model. The model contains two aquifers with water contents of 30 per cent separated by three layers with water contents of 5 per cent. The aquifers have thicknesses of 6 and 10 m located at depths of 4 and 25 m, respectively. A relaxation time of 500 ms is assigned to the aquifers, whereas the other layers have relaxation times of 100 ms. The C parameter is set to 0.7 for the aquifers, and to 0.9 for the other layers. The resistivity, ρ, is 100 ohm-m for all layers. The true model is shown in Fig. 6(c) by dashed red lines. The earth's magnetic field is set to 48 000 nT at an inclination of 60° and a declination of 0° (mid-Europe conditions). We have selected the pulse moment incremental values from one of the field data acquired by NUMIS Poly equipment (IRIS Instruments) so all parameters for calculation of the synthetic data are comparable with real-field conditions.

The forward response is contaminated by Gaussian noise with standard deviation of ∼40 nv (applied to the data before gating, at a sampling rate of 19200 Hz, and assuming the noise on the data to be uncorrelated), superimposed by 3 per cent of data values as uniform noise. This noise level was chosen to give meaning to the sensitivity analysis of the parameters and to evaluate the applicability of the proposed procedure for a real case scenario. Except for the layer resistivities, no *a priori* constraints have been imposed to the model parameters and layer thicknesses. The starting model is homogeneous with a resistivity of 100 ohm-m, a water content of 10 per cent, relaxation time of 200 ms and C = 1.0 for all layers. To show the ability of the inversion to retrieve the right layer thicknesses from only the variation of the stretched-exponential parameters, the resistivity values are fixed during the inversion.

Fig. 6(a) shows the fit to the data (black lines) on a logarithmic amplitude scale which represent very well the decay characteristics

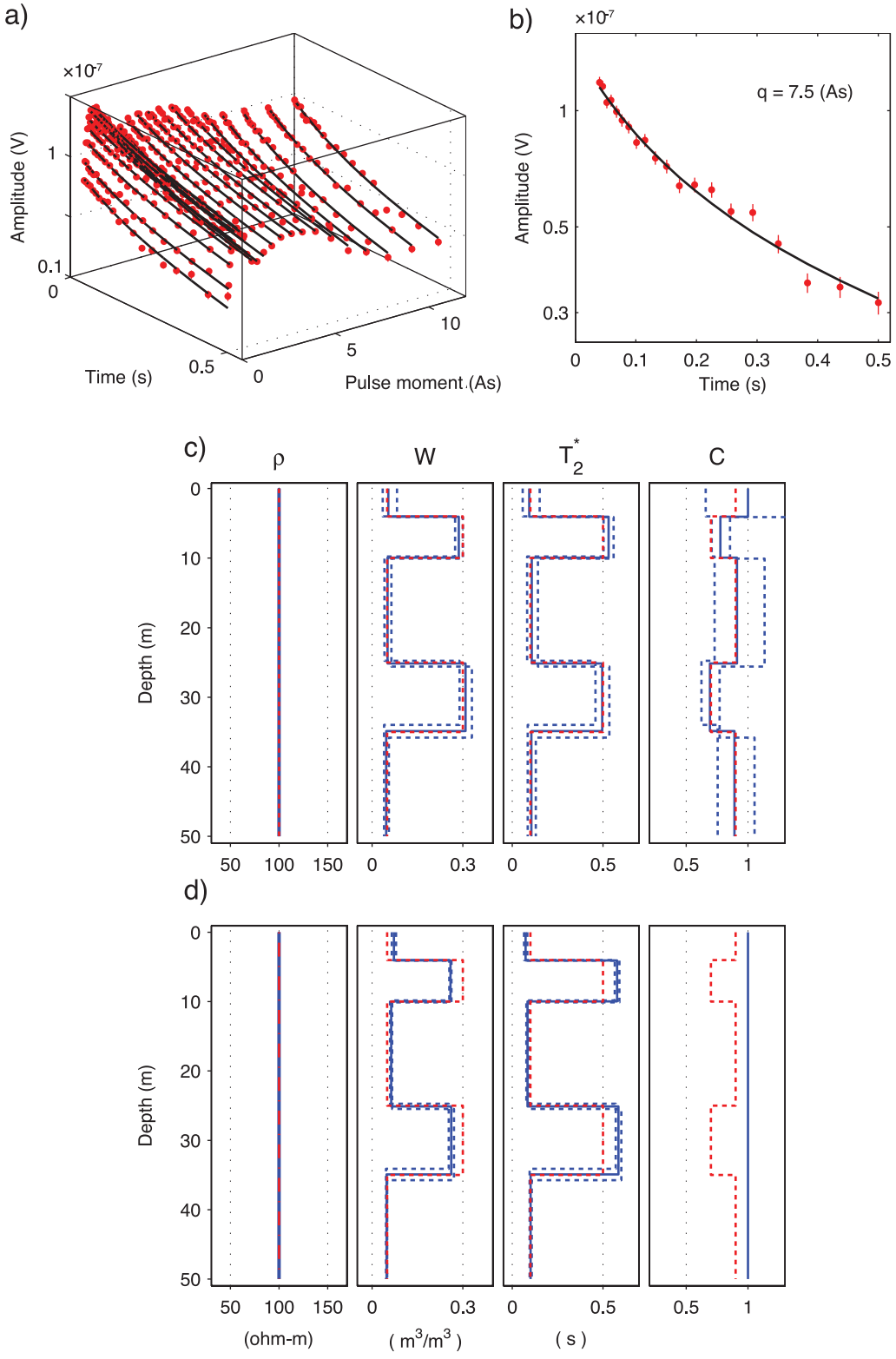

Figure 6. Synthetic example. (a) Synthetic MRS data set (red dots) together with the fit trough the data (black lines). (b) close-up view of one of the FIDs. (c) Synthetic model (dashed red lines) and inversion model (solid blue line), together with 68 per cent confidence interval (dashed blue lines). (d) The same as (c) except that the parameter C is constrained to one for inversion. A 50-m-side-square loop, and earth's magnetic field of 48 000 nT at inclination of 60° and declination of 0° were used. The model contains resistivity of 100 ohm-m (all layers), water contents of 5, 30, 5, 30 and 5 per cent, relaxation time of 100, 500, 100, 500 and 100 ms, the *C* parameter of 0.9,0.7,0.9,0.7 and 0.9, and thicknesses of 4, 6, 15 and 10, respectively from top to bottom.

of the FIDs. For better visualization, one of the FIDs is plotted separately in Fig. 6(b).

Eq. (18) was used to perform the sensitivity analysis of the model parameters. Because the model parameters are represented as logarithms, the analysis gives a standard deviation factor (STDF) on the parameter m_i defined by

$$\mathrm{STDF}\,(m_i) = \exp\left[\sqrt{C_{\mathrm{est}}(i,i)}\right]. \tag{19}$$

Therefore, under a lognormal assumption, it is 68 per cent likely that a given model parameter m falls in the interval

$$\frac{m}{\mathrm{STDF}_m} < m < m\mathrm{STDF}_m. \tag{20}$$

Fig. 6(c) shows the inversion results (solid blue lines) together with the corresponding synthetic model (dashed red lines) and the 68 per cent confidence intervals (dashed blue lines). All parameters are well resolved, and appropriate confidence intervals are obtained by the sensitivity analysis. Larger confidence intervals for the parameter C in the 1st, 3rd and 5th layers is expected due to low water content and small relaxation time of these layers.

To study the effect of the simplified description of the model using mono-exponential fit through the data, the inverse problem is solved for the same model response but fixing the C parameter to 1 for all layers. As Fig. 6(d) shows, the aquifer water contents are underestimated at 25.9 and 26.2 per cent and the relaxation times are overestimed at 578 and 586 ms. Also, Fig. 6(d) shows that the true parameter values of the aquifers have fallen outside the confidence interval, due to the insufficient forward description.

FIELD EXAMPLE

We will show the results from a MRS survey near Oksbøl in Denmark to evaluate the inversion scheme. The survey was carried out with a NUMIS Poly equipment (IRIS Instruments) using a 50-m-side-square loop with one turn. The earth's magnetic field had an intensity of 50 100 nT at an inclination of 70° and a declination of +2°. The MRS measurements consisted of 24 pulse moments, ranging from 0.12 to 14.0 As. The resistivity information are taken from TEM data aquired by a ground-based TEM instrument (40 m × 40 m square transmitter loop, central loop configuration).

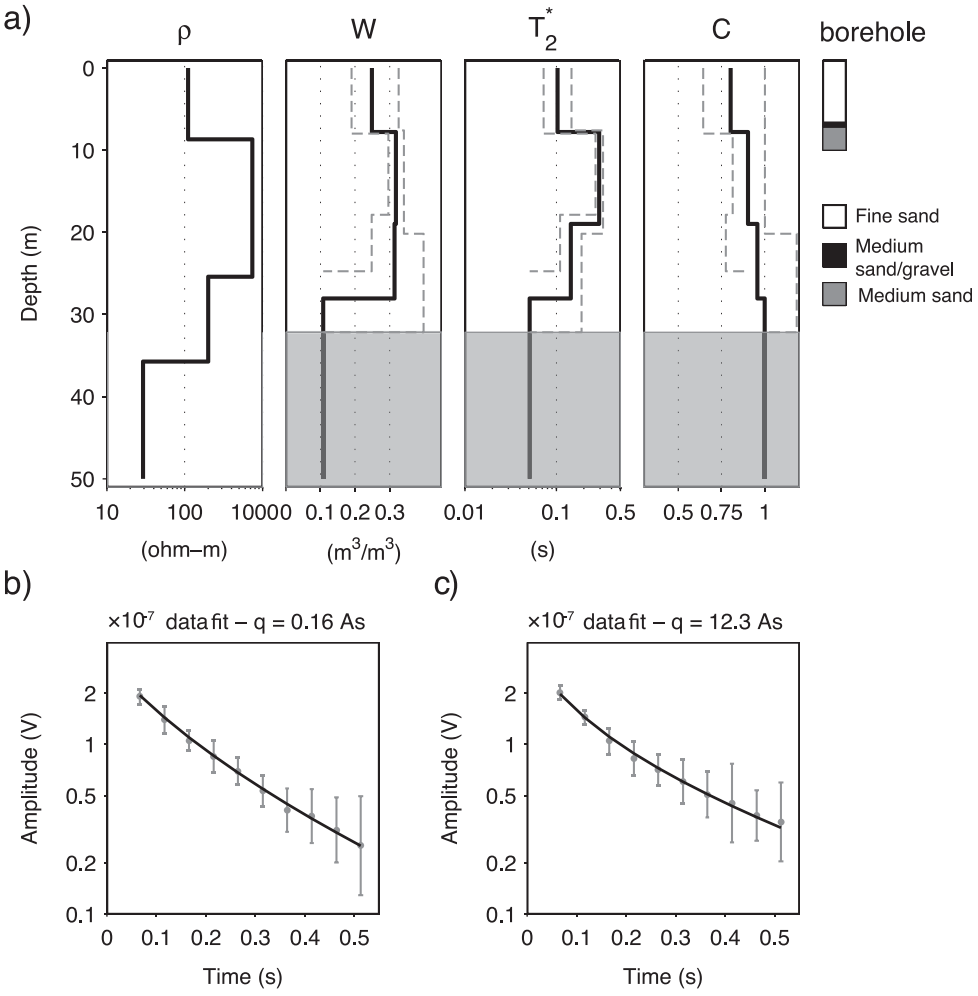

Figure 7. Inversion results of the field data. (a) Inversion results (solid black lines) and confidence intervals (dashed grey lines). Shaded grey boxes represent weak sensitivity information of the parameters of the last layer. The information of a borehole at the sounding position is shown as a column bar. (b) and (c) The fit through two of the FIDs at low (b, $q = 0.16$ As) and high (c, $q = 12.3$ As) pulse moments. Grey dots show the observed data, together with their standard deviation, and black lines represent the model response. The data was acquired using a 50-m-side-square loop, one turn in the earth's magnetic field intensity of 50 100 nT at an inclination of 70° and a declination of +2°.

Fig. 7(a) shows the inversion results. Resistivity values of 111, 742, 200 and 29 ohm-m were found as a result of inversion of the TEM data and imposed as fixed *a priori* constraints as depicted in column 1 in Fig. 7(a). Except resistivities, no *a priori* constraints are applied to the model parameters and layer thicknesses. The starting model for the few layer inversion was obtained based on a smooth inversion of the data in which the layer thicknesses do not change during the inversion and a vertical smoothing constraint is imposed on the model parameters. Solid black lines show the inversion model and dashed grey lines represent the 68 per cent confidence intervals. The inversion result has a first layer containing 25 per cent of water and relaxation time of 100 ms. This layer is underlain by two layers with water contents of 32 and 31 per cent. Compared to layer one, layer two has higher water content and a significantly higher relaxation time of 294 ms, which indicates larger pore size distribution. The first two layers agree well the information from a borehole located at the sounding (Fig. 7a). The first layer is fine sand, whereas the second layer is medium sand and some gravel. The presented field example is an example for which layers two and three cannot be distinguished based on water content distribution (assuming inversion of initial amplitudes only). In contrast, full decay inversion of the data introduces a decrease in the relaxation time of the third layer (144 ms) compared to the relaxation time of the second layer. The bottom layer is shaded grey to indicate weak sensitivity information of the parameters (parameter STDF of above 2). The rest of the parameters are well resolved. C values of 0.80, 0.90, 0.96 and 1.00 are found for the four layers, respectively.

The fit to two of the FIDs at low ($q = 0.16$ As) and high ($q = 12.3$ As) pulse moments are shown in Figs 7(b) and (c) on a logarithmic scale. Grey dots are the observed data, together with their standard deviation, and the black lines represent the model response. The data fit is well within the noise level.

CONCLUSION AND DISCUSSION

We have introduced a new approach for inversion of MRS data that includes the full MRS data set. The multi-exponential behaviour of the MRS signal is approximated by the stretched-exponential approach, which provides a simple description of the signal relaxation, and takes the spectral information of the relaxation distributions into account. We have described the assumptions for using the *SE* approach in MRS applications under which the approach provides an acceptable approximation of the complex decay behaviour.

The solution to the numerical issues implemented in this study, with respect to magnetic field computation, discretization and integration, have proven to be efficient. We have used a piecewise linear loop for EM modelling of conductivities, which means that an arbitrary shaped loop can be modelled accurately. This is one of the advantages of the presented approach compared to other existing routines. The accuracy of the discretizetion and integration scheme is validated against reference models revealing an accuracy better than 1 per cent. The forward response is compared with three other codes, showing close agreement with one code, and larger differences to two other codes.

The inversion scheme employs a smaller model space using the *SE* approach, compared to the multi-exponential approach. Moreover, a smaller data space is achieved using gate integration. The scheme has been examined by synthetic data superimposed by a noise level comparable to the real noise in the field, in which all model parameters are well resolved. The results of a field example agree well with borehole information, and the model response fits the entire data set well. The results show an example where the water content is constant over two layers having varying relaxation times. In this case, the inversion of the full data set was crucial for an accurate model output.

The inversion algorithm presented in this paper has been implemented in the em1dinv code (Christiansen & Auken 2008), that handles several electrical and electromagnetic methods in the same framework, and it is free for the scientific community.

Future work

The following issues are beyond the scope of this paper and among the future work on understanding of surface-NMR.

(1) The sensitivity kernel has been calculated under on-resonance condition as expressed by eq. (2). However, perfect on-resonance measurement is not realizable in the field due to, for example, temporal variation of the earth's magnetic field and magnetic susceptibility of the subsurface. Frequency offset produces a phase shift in addition to the one due to conductivity structure of the subsurface (Legchenko 2004; Walbrecker *et al*. 2011). Walbrecker *et al*. (2011) have studied off-resonance effects in surface-NMR, and highlighted that its effects cause biased results, particularly in double-pulse experiment. Therefore, it should be modelled in the forward calculation.

(2) The inversion results presented here are obtained by using the (rotated) amplitude of the signal (Mueller-Petke *et al*. 2011). The use of both real and imaginary parts of the data improves the inversion results (Legchenko 2004; Braun *et al*. 2005). Therefore, the correct estimation of the phase characteristics of the FIDs should be investigated and included in the inversion scheme.

(3) The forward response supports arbitrary loop shapes. The discretization scheme used in this paper can be generalized so that the magnetic fields of any loop geometry are calculated throughout a discretization system, which is independent of loop shape (e.g. Iron *et al.* 2010; Lehmann-Horn *et al*. 2011).

ACKNOWLEDGMENTS

This work was supported by the Danish Agency for Science Technology and Innovation funded project RiskPoint (Assessing the risks posed by point source contamination to groundwater and surface water resources) under grant number 09–063216. We thank James Ramm, Aarhus University, for his help in the field. Esben Dalgaard, University of Aarhus, processed the field data. We would also like to thank two anonymous reviewers and the associate editor whose constructive and fruitful comments helped improve the clarity of this paper.

REFERENCES

Apitz, D. & Johansen, P.M., 2005. Limitations of the stretched exponential function for describing dynamics in disordered solid materials, *J. appl. Phys.,* **97,** 1–4.

Auken, E. & Christiansen, A.V., 2004. Layered and laterally constrained 2D inversion of resistivity data, *Geophysics,* **69,** 752–761.

Becker, A. & Cheng, G., 1988. Detection of repetitive electromagnetic signals, in *Electromagnetic Methods in Applied Geophysics,* Volume 1, Theory, ed. Nabighian, M.N., Society of Exploration Geophysicists (SEG), Tulsa, OK, doi:10.1190/1.9781560802631.ch7.

Borgia, G.C., Bortolotti, V., Brancolini, A., Brown, R.J.S. & Fantazzini, P., 1996. Developments in core analysis by NMR measurements, *Magn. Reson. Imaging,* **14,** 751–760.

Braun, M., Hertrich, M. & Yaramanci, U., 2005. Study on complex inversion of magnetic resonance sounding signals, *Near Surface Geophys.,* **3,** 155–163.

Christiansen, A.V. & Auken, E., 2008. Presenting a free, highly flexible inversion code *SEG Expanded Abstr.,* **27,** 1228–1232, doi:10.1190/1.3059140.

Christiansen, A.V., Auken, E. & Viezzoli, A., 2011. Quantification of modeling errors in airborne TEM caused by inaccurate system description, *Geophysics,* **76,** f43–f52.

Dunn, K.J., Bergman, D.J. & Latorraca, G.A., 2002. *Nuclear Magnetic Resonance—Petrophysical and Logging Applications,* Pergamon Press, Oxford.

Forsythe, G.E., Malcolm, M.A. & Moler, C.B., 1977. Interpolation, in *Computer Methods for Mathematical Computations,* Prentice-Hall, New Jersey, NJ.

Hertrich, M., 2008. Imaging of groundwater with nuclear magnetic resonance, *Prog. Nucl. Magn. Reson. Spectrosc.,* **53,** 227–248.

Hilfer, R., 2002. Analytical representations for relaxation functions of glasses, *J. Non-Cryst. Solids,* **305,** 122–126.

Irons, T., Yaoguo, L. & McKenna, J.R., 2010. Frequency domain surface nuclear magnetic resonance forward modeling on an adaptive octree mesh, *SEG Expanded Abstr.,* **29,** 3935–3939, doi:10.1190/1.3513671.

Kenyon, W.E., 1997. Petrophysical principles of applications of NMR logging, *Log Anal.,* **38,** 21–40.

Kenyon, W.E., Day, P.I., Straley, C. & Willemsen, J.F., 1986. Compact and consistent representation of rock NMR data for permeability estimation, in *Proceedings of the 61st Annual Technical Conference and Exhibition of the Society of Petroleum Engineers,* Paper SPE 15 643, Society of Petroleum Engineers, Richardson, TX.

Kenyon, W.E., Day, P.I., Straley, C. & Willemsen, J.F., 1988. Three-part study of NMR longitudinal relaxation properties of water-saturated sandstones, *SPE Form. Eval.,* **3,** 622–636.

Legchenko, A., 2004. Magnetic resonance sounding: enhanced modeling of a phase shift, *Appl. Magn. Reson.,* **25,** 621–636.

Legchenko, A., Baltassat, J.M., Beauce, A. & Bernard, J., 2002. Nuclear magnetic resonance as a geophysical tool for hydrogeologists, *J. Appl. Geophys.,* **50,** 21–46.

Legchenko, A. & Valla, P., 2002. A review of the basic principles for proton magnetic resonance sounding measurements, *J. appl. Geophys.,* **50,** 3–19.

Legchenko, A.V. & Shushakov, O.A., 1998. Inversion of surface NMR data, *Geophysics,* **63,** 75–84.

Lehmann-Horn, J.A., Hertrich, M., Greenhalgh, S. & Green, A.G., 2011. Three-dimensional magnetic field and nmr sensitivity computations incorporating conductivity anomalies and variable-surface topography, *IEEE Trans. Geosci. Remote Sens.,* **49**(10), 3878–3891.

Marquart, D., 1963. An algorithm for least squares estimation of nonlinear parameters: SIAM, *J. appl. Math.,* **11,** 431–441.

Mohnke, O. & Yaramanci, U., 2005. Forward modeling and inversion of MRS relaxation signals using multi-exponential decomposition, *Near Surface Geophys.,* **3,** 165–185.

Mohnke, O. & Yaramanci, U., 2008. Pore size distributions and hydraulic conductivities of rocks derived from Magnetic Resonance Sounding relaxation data using multi-exponential decay time inversion, *J. appl. Geophys.,* **66,** 73–81.

Mueller-Petke, M., Dlugosch, R. & Yaramanci, U., 2011. Evaluation of surface nuclear magnetic resonance-estimated subsurface water content, *New J. Phys.,* **13,** 165–185.

Mueller-Petke, M. & Yaramanci, U., 2010. QT inversion—comprehensive use of the complete surface NMR data set, *Geophysics,* **75,** WA199–WA209.

Packard, M. & Varian, R., 1954. Free nuclear induction in the earth's magnetic field, *Phys. Rev.,* **93,** 941.

Peyron, M., Pierens, G.K., Lucas, A.J., Hall, L.D. & Stewart, R.C., 1996. The modified stretched-exponential model for characterization of NMR relaxation in porous media, *J. Magn. Reson.—Ser. A,* **118,** 214–220.

Phillips, J.C., 1996. Stretched exponential relaxation in molecular and electronic glasses, *Rep. Prog. Phys.,* **59,** 1133–1207.

Tarantola, A. & Valette, B., 1982a. Generalized nonlinear inverse problems solved using a least squares criterion, *Rev. Geophys. Space Phys.,* **20,** 219–232.

Tarantola, A. & Valette, B., 1982b. Inverse problems = quest for information, *J. Geophys.,* **50,** 159–170.

Walbrecker, J.O., Hertrich, M. & Green, A.G., 2011. Off-resonance effects in surface nuclear magnetic resonance, *Geophysics,* **76,** G1–G12.

Wannamaker, P.E., Hohmann, G.W. & SanFilipo, W.A., 1984. Electromagnetic modeling of three-dimensional bodies in layered earths using integral equations, *Geophysics,* **49,** 60–74.

Ward, S.H. & Hohmann, G.W., 1988. Electromagnetic theory for geophysical applications, in *Electromagnetic Methods in Applied Geophysics,* Volume 1, Theory, ed. Nabighian, M.N., Society of Exploration Geophysicists, Tulsa, OK, doi:10.1190/1.9781560802631.ch4.

Weichman, P.B., Lavely, E.M. & Ritzwoller, M.H., 2000. Theory of surface nuclear magnetic resonance with applications to geophysical imaging problems, *Phys. Rev.,* **62,** 1290–1312.

Xiong, Z., 1989. Electromagnetic fields of electric dipoles embedded in a stratified anisotropic earth, *Geophysics,* **54,** 1643–1646.